Form Approved
OMB NO. 0704-0188

1. AGENCY USE ONLY (Leave Blank)	2. REPORT DATE	3. REPORT TYPE AND DATES COVERED
	Feb. 25, 2007	Final report 10-1-2003 to 9-30-2006

4. TITLE AND SUBTITLE
Dilute-nitride type-II quantum well lasers grown by MOCVD

5. FUNDING NUMBERS
DAAD 19-03-1-0367

6. AUTHOR(S)
Luke J. Mawst

7. PERFORMING ORGANIZATION NAME(S) AND ADDRESS(ES)
University of Wisconsin-Madison

8. PERFORMING ORGANIZATION REPORT NUMBER

9. SPONSORING / MONITORING AGENCY NAME(S) AND ADDRESS(ES)
U. S. Army Research Office
P.O. Box 12211
Research Triangle Park, NC 27709-2211

10. SPONSORING / MONITORING AGENCY REPORT NUMBER
45572.2-EL

11. SUPPLEMENTARY NOTES
The views, opinions and/or findings contained in this report are those of the author(s) and should not be construed as an official Department of the Army position, policy or decision, unless so designated by other documentation.

12 a. DISTRIBUTION / AVAILABILITY STATEMENT
Approved for public release; distribution unlimited.

12 b. DISTRIBUTION CODE

13. ABSTRACT (Maximum 200 words)

One challenging goal remaining for GaAs-based InGaAsN QW lasers is to extend the emission wavelength beyond 1.3 •m, while maintaining optical material quality for the realization of longer wavelength and high performance. Higher N-content leads to increased nonradiative monomolecular recombination, thus high performance at 1.55 •m has not been achieved to date. Recently, we proposed a novel approach for realizing GaAs-based diode lasers with emission wavelengths beyond •=1500 nm. This approach utilizes the type-II band alignment between InGaAsN and GaAsSb. The PL emission wavelengths of previous InGaAs-GaAsSb type-II QW lasers, were generally limited to 1200-1400 nm, mainly due to strain limitations and the larger bandgap of InGaAs.

We have performed design studies using the 10-band k.p method to determine the compositional dependences of the optical matrix element and emission wavelength corresponding to the type-II transition. Increasing the In and Sb contents both extend the emission wavelength, due to reduced bandgap for the corresponding layers.

The dilute-nitride type-II laser structures reported here were grown by metalorganic chemical vapor deposition (MOCVD), at an active region growth temperature of 530 •C and reactor pressure of 100 mbar. 3-stage In0.37Ga0.62As0.98N0.02-GaAs0.7Sb0.3 "W" QW laser were fabricated and characterized

14. SUBJECT TERMS	15. NUMBER OF PAGES
	16. PRICE CODE

17. SECURITY CLASSIFICATION OR REPORT	18. SECURITY CLASSIFICATION ON THIS PAGE	19. SECURITY CLASSIFICATION OF ABSTRACT	20. LIMITATION OF ABSTRACT
UNCLASSIFIED	**UNCLASSIFIED**	**UNCLASSIFIED**	**UL**

NSN 7540-01-280-5500

Standard Form 298 (Rev.2-89)
Prescribed by ANSI Std. 239-18
298-102

Table of Contents

Statement of Problem Studied

Investigate the properties of Dilute-nitride material grown by MOCVD for implementation into type-II quantum wells. Investigate diode laser characteristics employing type-II quantum wells. Investigate the wavelength limitations on dilute-nitride type-II quantum wells and complete a design study.

Program goals and Key developments

The overall goal of this program is to develop high performance long wavelength lasers on GaAs substrates. We are taking two approaches to the device design:

1. GaAsN/GaAsSb type-II strain compensated active regions
2. InGaAsN/GaAsSb type-II active regions

During the second year of this project we have made significant milestones on the path to developing these sources. The growth of these materials was quite challenging. However, the successful growth of these novel type-II structures allowed us to study the optical transitions in these materials and the role of nonradiative processes. Key developments this year are described in detail below and the figure numbers refer to the figures in the attachment **(see attachment)**.

Key results for 2005:

1. Achievement of high Sb content (Sb~40%) GaAsSb/GaAsN QW structures. Using very high Sb/As gas phase ratio or triethylantimony (TESb) as a source, we have demonstrated higher Sb incorporation during the second year. Structures with higher Sb content allow for structure designs targeting longer wavelength.
2. Achievement of InGaAsN/GaAsSb type-II structures with emission wavelengths as long as 1.6 μm at RT. Implementation of strain compensating GaAsP barriers which improve PL intensity.
3. Correlation of type-II emission wavelength with 10-band k*p simulation. Identified issues with comparing dilute-nitride compounds with the simulation.
4. Identification of optimal annealing and cooldown conditions for maximum PL intensity. A nitrogen cooldown after growth yields the highest PL inensity and is attributed to a reduction of hydrogen incorporation in the dilute-nitride material.
5. Fabrication and characterization of the first broad area laser structures with the type-II dilute-nitride active regions. Initial devices operate on a type-II transition, although exhibit a blue shifted wavelength compared with PL intensity. This is believed to be due to a combination of charge separation (internal electric fields) and gain contributions from higher-order n=2 transitions. Device optimization issues are discussed below and include the use of thicker quantum well layers and longer cavity devices (i.e. lower threshold carrier density).

I. GaAsN/GaAsSb type-II structures:

Studies of the MOCVD growth and optical characteristics of GaAsN/GaAsSb type-II QW structures have been carried out. Emission wavelengths near 1.5 μm are measured from room temperature photoluminescence (PL), demonstrating the type-II nature of the transition. We find good agreement of the PL peak wavelength with simulation studies using a 10-band k*p formalism. The k*p simulation code, developed at NRL, has now been transferred to UW-Madison for use in this program. We are now using this simulation code to optimize the device design and correlate experimental

results with structure changes. The importance of the thermal annealing conditions on room temperature luminescence intensity is also established.

Growth conditions: GaAsSb and GaAsN layers were grown in a horizontal MOCVD reactor operated at 78 Torr. Trimethyl gallium (TMGa), trimethyl antimony (TMSb), dimethyl hydrazine (DMHz) and arsine were used as the Ga, Sb, N and As precursors respectively in Pd-diffused H_2 carrier gas. Semi-insulating (SI) epi-ready GaAs (100) wafers without an intentional miscut were used as the substrate. The substrates were annealed in arsine at 650°C for 10 minutes to desorb any surface oxides prior to the growth. The temperature was subsequently ramped down to the growth temperature of 530°C under an arsine environment. A 30 nm thick initial layer of GaAs was grown before the alloy-layer growth. Thick layers of GaAsN were grown at V/III ratio of 740 with N/V ratio of 0.89. The thick layer samples were characterized using on-axis (400) x-ray diffraction (XRD) Θ-2Θ scans and off-axis (311) reciprocal space mapping to determine the strain state and the composition of the GaAsN layers. Electron Microprobe Analysis (EPMA) was also carried out to determine N concentration in the thick layers. The As/III ratio was then decreased in a stepwise manner to achieve desired N concentrations in the GaAsN films. Four-period pseudomorphic GaAs-GaAsN superlattices (SL) were grown under varying As/III ratio. The growth time for GaAs layer was 34 s while that for GaAsN was 8 s. Θ-2Θ XRD scans around (400) substrate peak were obtained and the SL peaks were fitted to a dynamical simulations model to determine the layer thickness and N concentration. This thickness and N concentration information was used calibrate the growth rate and compositions of GaAsN layers. A V/III ratio of 684 with N/V ratio of 0.96, resulting into 2.3 % of N in the films was chosen for the growth of GaAsN/GaAsSb type II superlattice.

The pseudomorphic GaAsSb layer in the type-II MQW structure was grown at a V/III ratio of 3.8 with Sb/V ratio of 0.8, resulting in 20% Sb incorporation. The gas switching sequence was optimized to produce the most abrupt interfaces between the alloy layers. The gas switching sequence consisted of 5 seconds of TMSb and H_2 exposure prior to GaAsSb layer growth and 1 second of TMGa in H_2 followed by 5 seconds of arsine and DMHz exposure prior to the GaAsN layer growth. For thin pseudomorphic GaAs-GaAsSb SL layers with 20% Sb, the optimal gas-switching sequence that reproducibly induced minimal Sb compositional grading was established in a separate study [16].

Four periods of $GaAs_{0.78}Sb_{0.022}/GaAs_{0.978}N_{0.022}$ type II SL with were grown at the above mentioned optimized growth conditions. XRD Θ-2Θ scans and dynamical simulations were used to determine the thickness and layer compositions. Transmission electron microscopy (TEM) was performed in cross-section to confirm the layer thickness. The samples were subjected to various post-growth annealing treatments, which consisted annealing under arsine- H_2 and N_2. The cool-down ambient after the arsine anneals was varied between arsine and H_2 and N_2. The as-grown and annealed samples were subjected to photoluminescence spectroscopy (PL) using cooled Ge detector with a lock-in amplifier.

A pseudomorphic four-period GaAs-GaAsN superlattice (SL) structure was grown at the same growth conditions. XRD Θ-2Θ scans were obtained from the SL sample and the SL peaks were fitted to dynamical simulation for the structure to

determine individual layer thickness. Samples grown with decreasing arsine flow to the reactor were found to have increasing N concentration in the GaAsN films. **FIG. 1** shows experimental and the fitted dynamical simulation Θ-2Θ scans for a GaAs-GaAsN SL structure grown at a V/III ratio of 665 and N/V ratio of 0.99. Presence of second and higher order diffraction peaks indicated that the interfaces between the layers were uniform and smooth. Layer thickness and N concentration of GaAsN were determined from the fit to be 0.027% and 1.9 nm, respectively.

For the type-II GaAsN-GaAsSb SL structure, $GaAs_{0.978}N_{0.022}$ layers were grown at V/III ratio of 685 with N/V ratio of 0.96. **FIG. 2** shows the experimental and dynamical simulation XRD Θ-2Θ scans for a four period $GaAs_{0.978}N_{0.022}$-$GaAs_{0.78}Sb_{0.22}$ SL sample. The growth time for GaAsN layer was 18 seconds, whereas GaAsSb layer was grown for 53 seconds. The model fitted to the x-ray data indicated the layer thickness of $GaAs_{0.8}Sb_{0.21}$ and $GaAs_{0.978}N_{0.022}$ to be 4.5 and 7.5 nm, respectively. Cross-sectional bright field strain-contrast image from the GaAsN-GaAsSb sample is depicted in **FIG. 3**. Average layer thickness for GaAsN and GaAsSb layers determined from six TEM images were found to match closely with XRD derived thickness values. Considerable non-uniformity with respect to layer thickness was observed across each wafer and among different growth runs. The GaAsSb thickness ranged between 4.8 and 5.9 nm, whereas the GaAsN thickness varied from 5.9 to 8.3 nm across different runs.

30K photoluminescence (PL) spectra obtained from as-grown and annealed SL sample with 8 nm GaAs-2 nm $GaAs_{0.984}N_{0.016}$ layers are depicted in **FIG. 4**. The PL peak intensity increases two-fold after the annealing treatment, indicating small changes in the optical and electrical properties of the alloy layer upon annealing. The QW energy for GaAs-$GaAs_{0.084}N_{0.016}$ type-I electronic transition was calculated assuming perfect valence band line-up between GaAs and GaAsN and approximate solution for electron energy states, to be 1.44 eV, which matches up well with experimental peak energy of 1.39 eV. PL spectra obtained from the 5.7 nm $GaAs_{0.978}N_{0.022}$/4.3 nm $GaAs_{0.785}Sb_{0.215}$ type II SL sample is shown in **FIG. 5.** The 'annealed' spectrum was obtained from the sample after a 30 minute anneal at 640°C in arsine-H_2 with a cool-down under N_2 ambient. The PL intensity is normalized to the same scale and the intensity normalization factor is shown adjacent to the spectra. A 70-fold increase in PL intensity was observed for this annealing treatment, whereas RTA at 500°C for 1 minute resulted in a 3-fold decrease in the PL intensity. No room temperature (RT) PL intensity could be obtained from any of the as-grown type-II SL samples. The RT luminescence spectrum from the type-II sample annealed under arsine-H2 with a N2 cool-down is shown is **FIG. 6**. The peak wavelength was found to be about 1425 nm.

Theoretical energy gaps derived from the 10-band **k·p** formalism were compared with the PL measurement results. The theoretical results for the type-II GaAsN/GaAsSb QW structures were in good agreement with experimental results, especially before the annealing treatment. For example, the energy gaps calculated for the structure of **FIG. 5** and **6** are 1419 and 1515 nm at temperatures of 30 and 300 K, respectively. Good agreement was also obtained for a series of type-II GaAs/GaAsSb SLs emitting at wavelengths in the 1.0-1.2 μm range [16]. Furthermore, the calculated energy gap of 1043 nm for a 6 nm $GaAs_{0.975}N_{0.025}$ QW surrounded by thick GaAs barriers reproduces closely the experimental PL peak. The simulated peak positions, taken together with the

PL data in FIG. 5 and 6, imply that the transition observed in the GaAsSb/GaAsN SL is indeed of type-II nature, *i.e.*, with staggered conduction and valence band edges

Remaining issues with GaAsN/GaAsSb type-II design:

1. We have recently employed triethylantimony and triethygallium (TEGa, TESb) as sources for the low temperature growth of GaAsSb. These metalorganic sources decompose at lower temperatures compared with the trimethyl- versions. As a result, we expect to be able to achieve higher Sb content films at the low growth temperatures employed. Initial growths of GaAsSb/GaAs SL structures do confirm the ability to grow 40% Sb content films, compared with 20% Sb content achieved with the trimethyl sources. We now plan to incorporate these higher Sb content GaAsSb into the type-II structures.
2. Utilize high temperature annealing to enhance radiative recombination. We have employed annealing temperatures as high as 720^{o}C and find improved luminescence properties. We expect even higher temperature annealing may be beneficial.

II. InGaAsN/GaAsSb type-II structures:

As an alternative approach to the GaAsN electron well for the type-II structure, we have also investigated the use of a quaternary InGaAsN electron well. The potential advantage of the quaternary well is that longer wavelength emission is possible with lower N content material. However, the challenges of this approach are the higher compressive strain of the composite "w" active region and the blueshift observed during high temperature annealing of InGaAsN.

Low temperature (30 K) long wavelength photoluminescence emission (λ=1400-1600 nm) from metalorganic chemical vapor deposition (MOCVD) grown InGaAsN-GaAsSb type-II "W" quantum-wells on GaAs substrates has been demonstrated. Thin layers (2-3 nm) and high antimony-content (30%) GaAsSb were utilized in this study for realizing satisfactory wave function overlap and long wavelength emission. Tensile strained GaAsP barriers effectively improve the material structural and luminescence properties of the compressive strained active region. Room temperature photoluminescence data show that the type-II QW design is a promising candidate for realizing long wavelength GaAs-based diode lasers beyond 1500 nm.

In this work, the InGaAsN and GaAsSb thicknesses are kept at 2-3 nm, the practical range proposed by our previous theoretical study. Tensile-strained barriers of $GaAs_{0.85}P_{0.15}$ have been employed to compensate the compressively-strained "W"-active region. This strain compensation design is especially desirable in multiple-stage structures for maximizing the laser modal gain. Optimization of the layer thickness and

tensile strain of the GaAsP barriers leads to significant improvements in both the photoluminescence (PL) intensity and the full width half maximum (FWHM). The samples grown for this study contain of a single "W"-active region located at the center of a 300-nm wide GaAs separate confinement heterostructure (SCH) region. Thin $Al_{0.65}Ga_{0.35}As$ top- and bottom-cladding layers (150 nm) are included for better carrier and optical confinement.

The structures were grown by metalorganic chemical vapor deposition (MOCVD) at an active region growth temperature of 530 °C and reactor pressure of 100 mbar. Trimethylgallium (TMGa), trimethylaluminum (TMAl) and trimethylindium (TMIn) were the group III precursors materials, and AsH_3, PH_3 trimethylantimony (TMSb) and U-dimethylhydrazine (U-DMHy) were the group V precursors. The solid phase material compositions of InGaAsN and GaAsSb were determined by high-resolution x-ray diffraction (HRXRD) experiments with the layer thickness information obtained from transmission electron microscope (TEM) images. For GaAsSb, a low V/III ratio of 1.34 (gas phase Sb/V=85%) was utilized, leading to the high antimony solid content of 30% that is essential for achieving long wavelength emission. The growth rate under this condition was calibrated to be 90 Å/min. The gas-switching scheme was studied previously and utilized here for achieving good GaAsSb interfaces. Rough and graded interfaces can greatly deteriorate the luminescence intensity from the type-II QW structure, due to the nature of the spatially-indirect transition. For InGaAsN, the indium-content was 37% and the gas phase N/V ratio was in the 0.994-0.996 range, corresponding to a nitrogen-content of approximately 2%. In general, we utilized a very small $[AsH_3]$/III ratio (<10) for growing InGaAsN to allow for sufficient nitrogen incorporation. To characterize the grown QW optical quality, room temperature and low temperature PL measurements (30 K) were conducted with an argon-ion laser ($\lambda \sim 514.5$ nm) as the excitation source. **Figure 7** shows the (0 0 4) x-ray ω-2θ diffraction pattern of a three-stage InGaAsN-GaAsSb "W"-structure. Between each stage, GaAs and tensile strained GaAsP were employed as barriers to separate the highly strained active regions. The two broad envelope modulations represent the diffraction peaks from the individual InGaAsN and GaAsSb layers, as pointed out in the figure. They overlap with the Pendellösung fringes, which result from the diffraction of the periodic layer structure, forming the x-ray diffraction pattern shown in **Fig. 7**. The distinct fringe pattern indicates good crystal and interface quality of the highly strained materials.

Fig. 9 shows the 30 K PL spectrum of three as-grown InGaAsN-GaAsSb type-II "W" QW structures with various nitrogen-contents in the InGaAsN. The InGaAsN thickness is fixed at 2.5 nm,. and the thickness of the $GaAs_{0.7}Sb_{0.3}$ layers is 2-nm. The N/V ratios for these three samples are 0.994, 0.995 and 0.996, and the corresponding emission wavelengths are 1425, 1480 and 1620 nm, respectively. Without nitrogen, the peak emission wavelength for the InGaAs-GaAsSb type-II QW at 30K is 1260 nm. With more than 2.2% nitrogen (N/V=0.996), the longest emission wavelength is extended to 1620 nm, indicating a significant red shift of 220 meV due to the nitrogen-induced bandgap bowing. The PL spectral FWHM is increased from 30 meV for the nitrogen-free sample to 78-88 meV for the samples with high nitrogen-content. The significant degradation of the PL intensity and FWHM for the 1620 nm sample is presumably due to onset of the three-dimensional growth mode under such an extremely high N/V ratio, which is further verified by the HRXRD experiments.

To confirm that the light emission is a result of electron-hole radiative recombination via the type-II transition, InGaAsN-GaAs single QW and GaAsSb-GaAs single QW structures (keeping the same material compositions and QW thickness as the layers in the "W"-structure) were grown with the N/V ratio equal to 0.995. Those two QW structures and the type-II QW were in-situ annealed at 640 °C for 25 minutes. The 30 K PL emission wavelengths for all three are shown in **Fig. 9**. The peak wavelengths for the InGaAsN and GaAsSb QWs are 1184 and 1080 nm, respectively, while the peak for the type-II "W" QW occurs near 1380 nm. The significant wavelength extension obtained for the InGaAsN-GaAsSb "W"-structure confirms that the transition in this active region is type-II. The emission wavelength of 1380-nm for the annealed sample is shorter than that measured for the as-grown sample (1480-nm), shown in **figure 8** due to the well-known blue-shift effect that occurs when InGaAsN is thermally annealed. In addition to the wavelength blueshift, the PL intensity of the annealed sample is six times higher than that of the as-grown sample. According to our energy band structure simulation by the 10-band k*p formalism, the calculated 30 K emission wavelengths of the InGaAsN-GaAs QW, GaAsSb-GaAs QW, and type-II "W" structure are 1050, 1090 and 1330 nm, respectively. That the predicted emission wavelengths for the samples containing InGaAsN layers are shorter than the experimental results may be due to atomic ordering in the InGaAsN, which is not accounted for in the simulation. Since the thermal annealing condition utilized here does not saturate the blue shift, a higher-temperature anneal may induce further blue shift and hence closer agreement with theory. In addition, graded InGaAsN-GaAsSb interfaces may also contribute to the deviation between theory and experiment.

This type-II QW structure also displayed long wavelength emission at room temperature. RT PL from InGaAsN-GaAsSb "W"-structures is shown in fig. 10 with comparison to simulation, indicating near 1500nm emission can be achieved. Room temperature PL spectrum of the InGaAsN-GaAsSb "W"-structure with N/V of 0.996 and annealed at 720 °C was also observed. Under high excitation power density (100 W/cm^2), the emission wavelength is near 1600 nm. The wavelength shift from 1580 nm at 30 K to 1600 nm at room temperature results from the combination of a red shift with increasing temperature and a blue shift at higher excitation power density (and higher carrier density in the QW). This room temperature PL result indicates that the type-II QW design is a promising candidate for realizing long wavelength GaAs-based diode lasers that emit beyond 1500 nm.

Remaining Issues with InGaAsN/GaAsSb type-II structures:

1. The high compressive strain of the composite "w" structure needs to be minimized. High resolution TEM images of the InGaAsN/GaAsSb type-II structures indicate layer nonuniformities and wavey interfaces, probably related to the high compressive strain. Lower strain structures can be accomplished by employing lower In content InGaAsN electron wells. We are now studying the design optimization and growth of these structures.

III. Initial device results:

Broad area lasers (100 μm-wide stripe devices) have been fabricated using the type-II active regions. Initial device characterization was carried out in a cryostat for variable temperature spectral measurements. We are also setting up an optical pumping measurement stage, although the initial devices described here are electrically driven.

The first three structures investigated contain InGaAsN/GaAsSb type-II active regions:

- **a-4967NSL: InGaAsN-GaAsSb (2.5 nm-5 nm) W-structure**
  - **InGaAsN: In=37%, N~1.5%, AsH3=2.4 sccm**
  - **GaAsSb: Sb/V=75%, V/III=1.52, Sb~20%**
  - **720 °C annealed for 25 min**
- **a-5094NSL: InGaAsN-GaAsSb (2.5 nm-2 nm) W-structure**
  - **InGaAsN: In=37%, N~2%, AsH3=1.92 sccm**
  - **GaAsSb: Sb/V=85%, V/III=1.34, Sb~30%**
  - **720 °C annealed for 25 min**
- **a-5210NSL: InGaAsN-GaAsSb (2.5 nm-2 nm) W-structure**
  - **InGaAsN: In=37%, N~2.2%, AsH3=1.6 sccm**
  - **GaAsSb: Sb/V=85%, V/III=1.34, Sb~30%**
  - **640 and 720 °C annealed for 25 min**
  - **GaAsP direct barrier**

In all three device structures (**Fig. 11-13**) we find EL emission which is blueshifted with respect to the spontaneous emission (measured by low excitation PL). This blue shift is probably a result of internal fields induced by the charge separation in the type-II structure. Similar results have been reported previously from InGaAs/GaAsSb type-II lasers on GaAs substrates. Optimized structure design, such as thicker layers and reduced threshold carrier density (i.e. lower threshold gain) are expected to minimize the blueshift. Note that InAs/GaSb type-II quantum well lasers on GaSb substrates have been demonstrated with minimal blueshift due to charge separation.

We also observe a high energy peak in the EL spectrum which grows in intensity and eventually reaches laser threshold. This behavior is not well understood and may be a result of higher order type-II transitions. We plan to measure the EL emission wavelength as a function of cavity length (i.e. threshold gain) and structure design (i.e. quantum well layer thickness). In addition, we are collaborating with researchers at NRL to include the effects of charge separation and high-order energy transitions in our laser design. These design optimization studies is expected to lead to active regions with minimized emission blue shift. Another possible cause for the high energy peak in the EL spectrum is an asymmetric interface. This has been postulated previously (H. Takasaki et al., J. Crystal Growth, vol. 227-228, pg. 294(2001)) for InGaAs/GaAsSb type-II structures on InP. Note that we have only observed the double-peak EL behavior in InGaAsN/GaAsSb structures, not GaAsN/GaAsSb. We are currently fabricating GaAsN/GaAsSb type-II broad area lasers to characterize the EL spectral behavior.

Year III.

Based on work in year II, we determined the areas to focus on which will allow for device optimization.

- Larger number of W-stages: lower carrier density at threshold $\Rightarrow$ reduce blue-shift
- Reduce structure strain $\Rightarrow$
  - Lower In-content InGaAsN
  - Thinner layer thickness: higher wavefunction overlap
  - Higher P-content GaAsP barriers
- Higher Sb content: improved hole confinement

– TEGa, TESb sources*⇒ demonstrated GaAs0.57Sb0.43

1. A detailed study was undertaken on the use of alternate MO sources for the growth of the GaAsSb hole well layers. **Fig. 14** shows that very high Sb content layers are achieved with abrupt interfaces. The details of this study were recently published (A.A. Khandekar**,** J.Y. Yeh, L.J. Mawst, Xueyan Song, S.E. Babcock and T.F. Kuech, "Growth of strained $GaAs_{1-y}Sb_y$ layers using metalorganic vapor phase epitaxy**",** *Journal of Crystal Growth,* In Press). Very long wavelength emission was observed (~1.8 microns) from W structures with high N contents (N~3-4%).
2. An experimental/simulation design study was undertaken to determine a more optimal W design for near 1.5 mm emission , *with the minimal amount of nitrogen*. As shown in **Fig. 15**, 4 different structures were grown and characterized with N~1%. The PL results, as shown in **Fig. 16**, are very encouraging and thermal annealing studies are underway.
3. Preliminary work on 8 stage InGaAsN/GaAsSb W structures has been carried out. Higher P-content barriers were found effective to allow a large number of stages (up to 8) to be grown with excellent surface morphology. The next step is to incorporate an optimal 8 stage active region into a laser diode structure.

Future work could focus on implementing the high-Sb content W structures with 4-8 stages into the diode laser active regions. Optimal annealing conditions may significantly improve the optical properties of these active regions. Recent work reported by W. Stolz et al., at Philips University indicates that unstabilized (i.e. no Arsine) annealing can remove microscopic strain fields in InGaAsN and significantly improve PL intensity. These reports did not evaluate the impact on actual device performance.

Publications

1. J.-Y. Yeh , L. J. Mawst, A. A. Khandekar, T. F. Kuech, I. Vurgaftman, J. R. Meyer, and N. Tansu, "Long Wavelength Emission of InGaAsN/GaAsSb Type-II "W" Quantum Wells", Appl. Phys. Lett. **88**, 051115 (2006).
2. J. Y. Yeh, L. J. Mawst, A.A. Khandekar, T.F. Kuech, I. Vurgaftman, J. R. Meyer, N. Tansu, " Characteristics of InGaAsN-GaASSb type-II "W" quantum wells", J. Crystal growth, vol. 287, 615(2006).
3. A.A. Khandekar**,** J.Y. Yeh, L.J. Mawst, Xueyan Song, S.E. Babcock and T.F. Kuech, "Growth of strained $GaAs_{1-y}Sb_y$ layers using metalorganic vapor phase epitaxy**",** *Journal of Crystal Growth,* In Press, Corrected Proof.
4. A. A. Khandekar, B. E. Hawkins, T.F. Kuech, J.Y.Yeh, L.J. Mawst J.R.Meyer, I. Vurgaftman, N. Tansu, "Characteristics of GaAsN/GaAsSb type-II quantum wells grown by metalorganic vapor phase epitaxy on GaAs substrates, J. Appl. Phys. 98, 123525(2005).
5. Characteristics of InGaAsN/GaAsSb Type-II "W" Quantum Wells", J.-Y. Yeh, L. J. Mawst, A. A. Khandekar, T. F. Kuech, J. R. Meyer, Vurgaftman, N. Tansu, **International Conference on Metalorganic Vapor Phase Deposition (ICMOVPE)**, June, 2005.
6. Characteristics of GaAsN/GaAsSb type-II MQWs grown on GaAs substrates grown by Metalorganic Vapor Phase Epitaxy, A. A. Khandekar, B. Hawkins, J. Yeh, L. J. Mawst, T. F. Kuech, **Electronic Materials Conference**, June 2005.
7. Characteristics of MOCVD grown InGaAs QDs embedded in GaAsP/InGaP matrix, N. Kim, L. J. Mawst, T. F. Kuech, M. Kanskar**, Electronic Materials Conference**, June 2005.
8. A. A. Khandekar; J. Yeh; L. J. Mawst; Xueyan Song; S. E. Babcock; T. F. Kuech, "Effects of Ga and Sb Precursor Chemistry on the Alloy Composition in Pseudomorphically Strained GaAsSb Films Grown via Metalorganic Vapor Phase Epitaxy**",** TMS Electronic Materials Conference", Pennsylvania, June 26, 2006.
9. Nelson Tansu**,** Jeng-Ya Yeh, and Luke J. Mawst, **"**Effect of Strain on the Nitrogen Incorporation in InGaAsN Quantum Wells Grown on GaAs and InP Substrates by Metalorganic Vapor Phase Epitaxy", TMS Electronic Materials Conference", Pennsylvania, June 26, 2006.
10. A. Khandekar, J. Y. Yeh, L. J. Mawst, J. R. Meyer, I. Vurgaftman, and N. Tansu and T. F. Kuech **, "**Effects of Ga and Sb Precursor Chemistry on the Alloy Composition in Pseudomorphically Strained GaAsSb Films Grown via Metalorganic Vapor Phase Epitaxy"**,** ICMOVPE 2006**,** Miyazaki, JAPAN, May 22, 2006.
11. L. J. Mawst , J. Y. Yeh , D. Xu , J. H. Park , Y. Huang, A. Khandekar , T. F. Kuech, N. Tansu , I. Vurgaftman , and J. R. Meyer, "InGaAsN/GaAsSb/GaAs(P) Type-II 'W' Quantum Well Lasers**",** CLEO 2006**,** Long Beach Convention Center, California, May 21, 2006

Graduate Students working on Program

1. Anish Khandekar, Ph.D. in Chemical Engineering May 2006
2. Jeng-Ya Yeh, Ph.D. in Electrical Engineering, Sept. 2005

Inventions

1. L. J. Mawst, N. Tansu, J. Yeh, “ Highly Strained InGaAs Qquantum wells with dilute-nitride based barriers for emission wavelength > 1.23 microns”, field with US Patent Office Dec. 2005.

Appendix: This file contains the figures referred to in the report text description

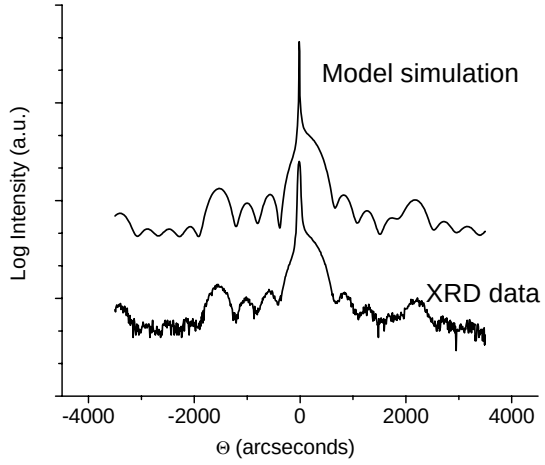

FIG. 1. XRD high-resolution Θ-2Θ scan around (400) Bragg peak and dynamical simulation for 8.4nm GaAs/1.9 nm $GaAs_{0.98}3N_{0.027}$ four-period SL

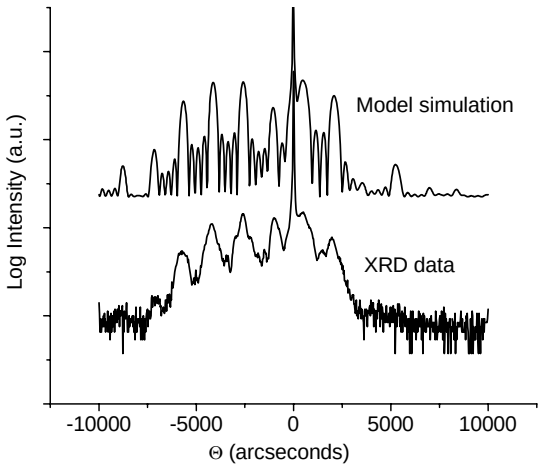

FIG. 2. XRD high-resolution Θ-2Θ scan around (400) Bragg peak and dynamical simulation for 4.9 nm $GaAs_{0.78}Sb_{0.22}$/7.2nm $GaAs_{0.978}N_{0.022}$ four-period SL

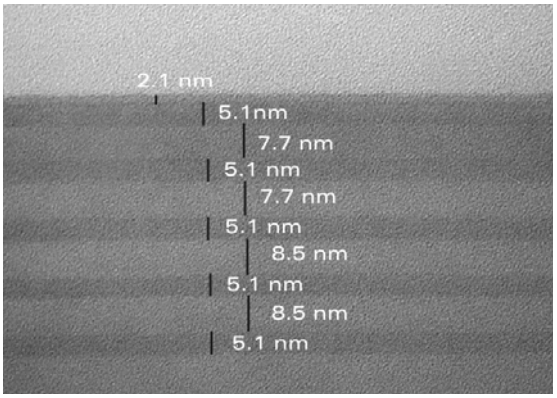

Fig. 3 Cross-sectional BF TEM micrograph for a 4.9 nm $GaAs_{0.79}Sb_{0.21}$/7.8 nm $GaAs_{0.978}N_{0.022}$ four-period SL sample

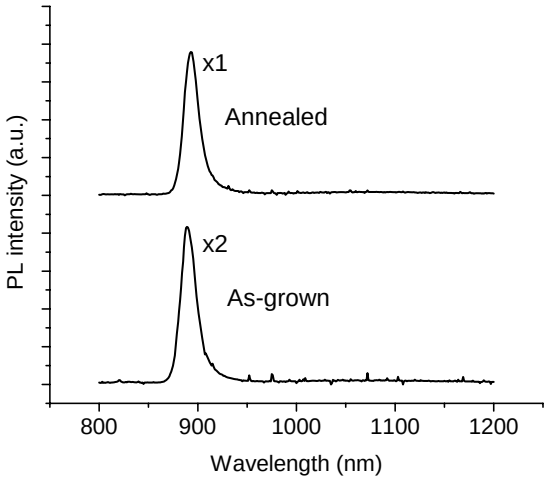

Fig. 4 Photoluminescence spectra from as-grown and annealed 8 nm GaAs/2 nm $GaAs_{0.084}N_{0.016}$ 4- period SL structure

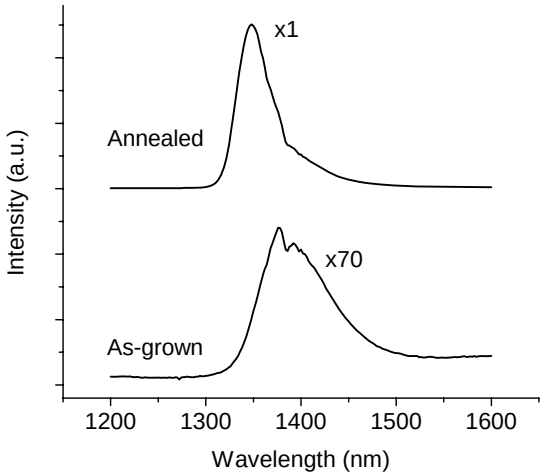

Fig. 5 30 K PL spectra from as-grown and annealed 5.7 nm $GaAs_{0.978}N_{0.022}$/4.3 nm $GaAs_{0.78}Sb_{0.22}$ four-period SL sample

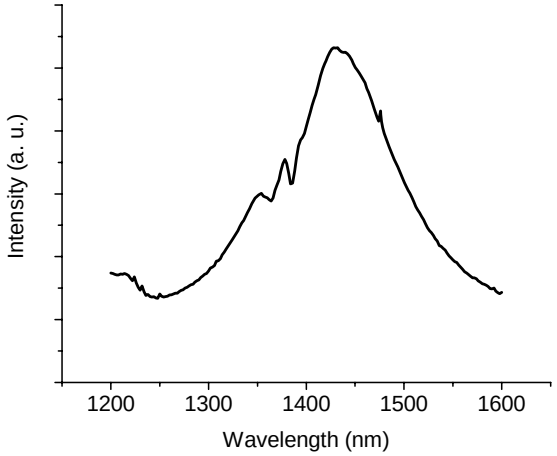

Fig. 6 Room temperature (300 K) PL spectra for the annealed GaAsSb/GaAsN four-period SL sample of FIG. 5.

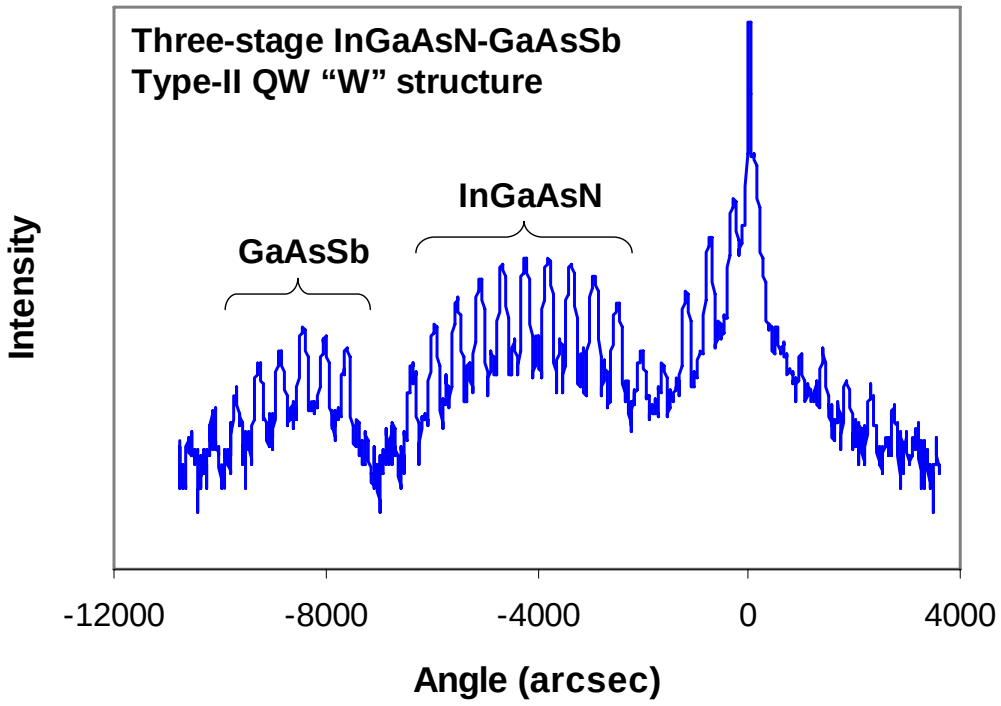

Fig. 7 The high-resolution x-ray ω-2θ diffraction pattern, along the (0 0 4) direction, for a three-stage InGaAsN-GaAsSb "W" structure. The two envelopes are induced by the GaAsSb and InGaAsN layers. The distinct fringe pattern confirms the high quality of the grown materials and interfaces, in spite of the large lattice mismatch (~2%).

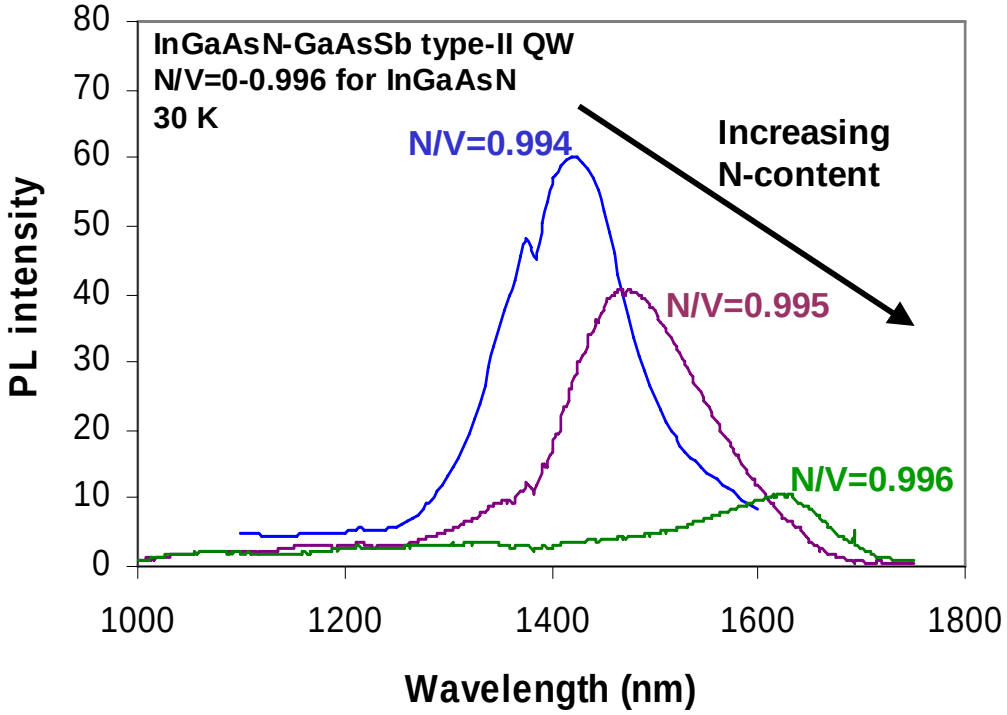

Fig. 8 30 K PL spectrum of the InGaAsN-GaAsSb type-II QW "W" structures grown with various gas phase N/V ratios ranging from 0.994 to 0.996. A substantial wavelength red shift was observed with increasing nitrogen-content in the InGaAsN QW.

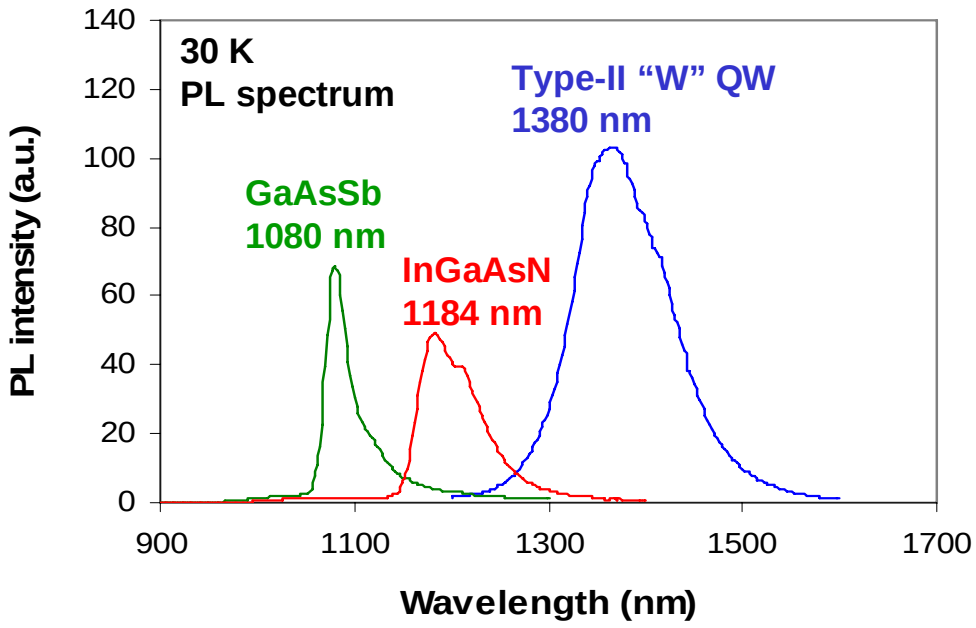

Fig. 9 PL comparison between the type-II structure and InGaAsN and GaAsSb type-I QWs, showing clear evidence for longer-wavelength emission when the type-II band alignment is employed.

Comparing Type-I and Type-II "W" QW*

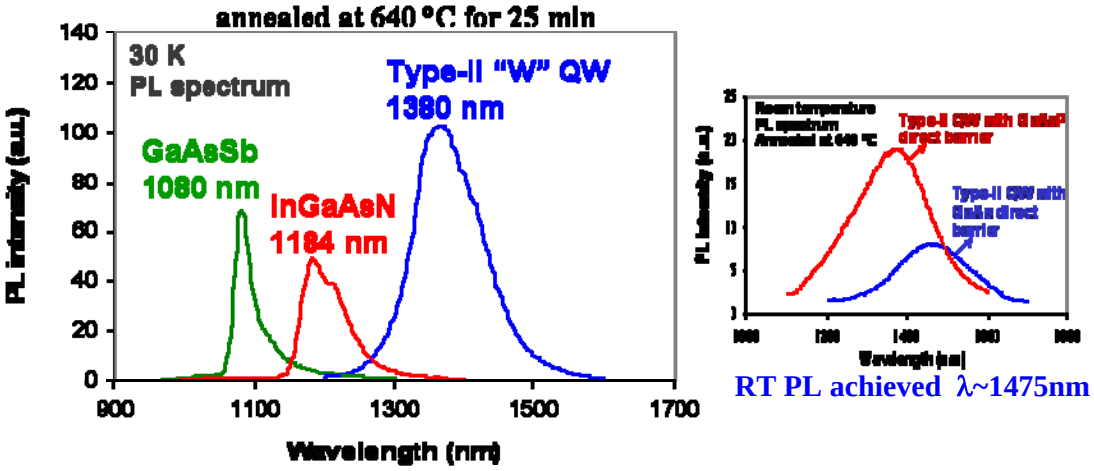

- 2.5 nm $In_{0.37}Ga_{0.63}As_{0.978}N_{0.022}$ SQW emits at 1184 nm⇒ simulated 1050nm
- 2 nm $GaAs_{0.7}Sb_{0.3}$ SQW emits at 1080 nm ⇒ simulated 1080nm
- Type II QW emits at λ~1380 nm ⇒ simulated 1345nm

* J.-Y. Yeh, et al., Appl. Phys. Lett., 2006.

Fig. 10 Room temperature (300 K) PL spectrum of the InGaAsN-GaAsSb type-II "W" structure.

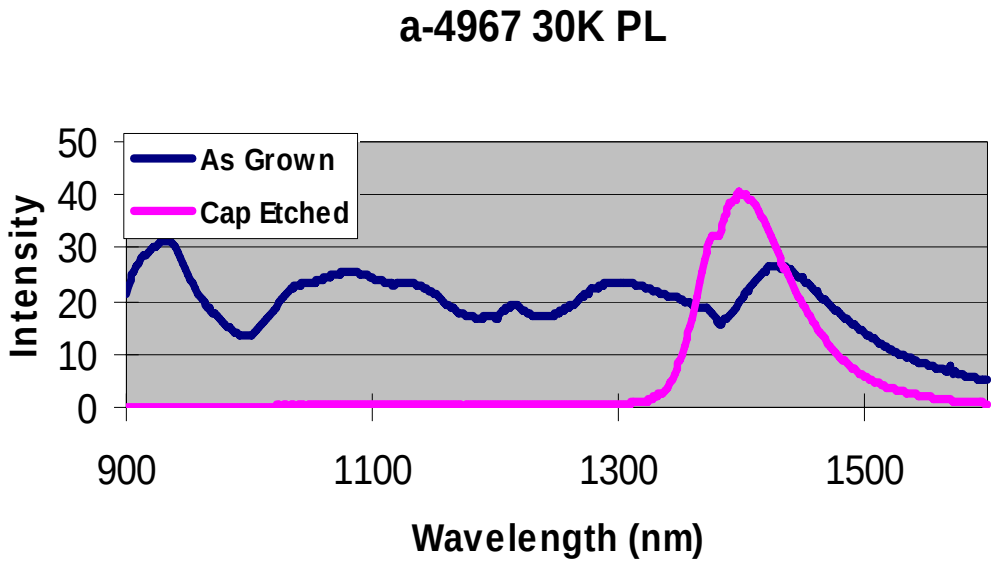

a)

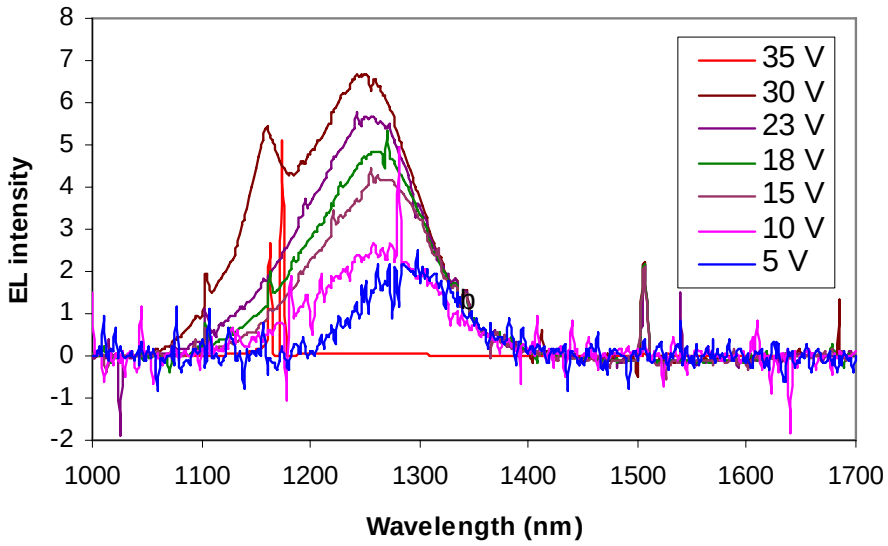

b)

Fig. 11 a) sample a-4967NSL 30K PL emission and b) 30K EL emission at various drive currents.

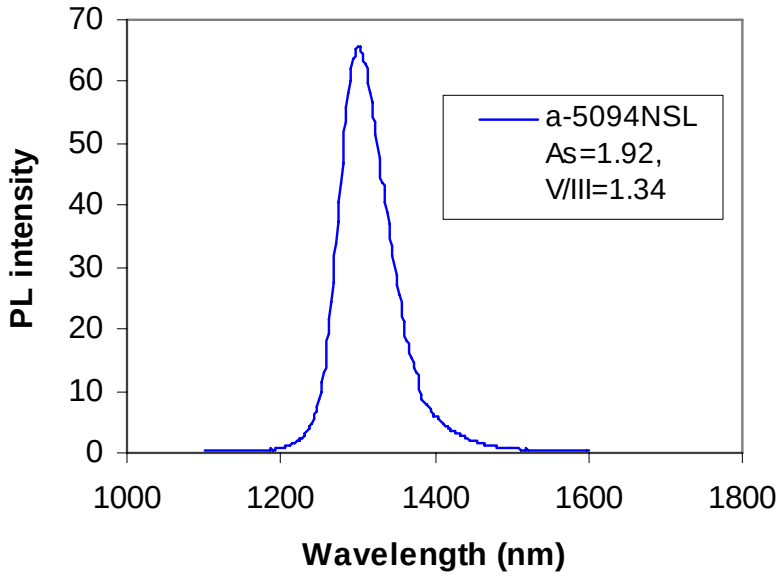

a)

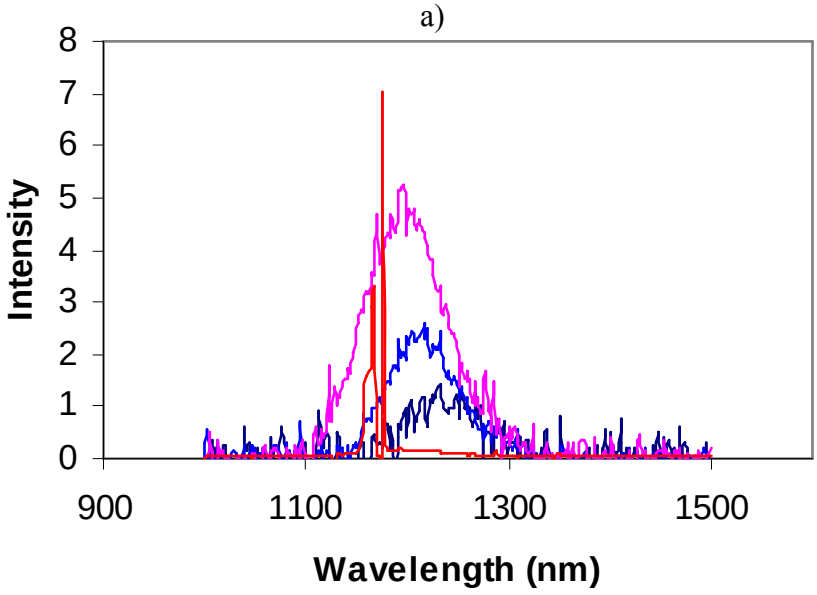

b)

Fig. 12 a) sample a-5094NSL 30K PL and b) 30K EL showing lasing near 1.2 μm

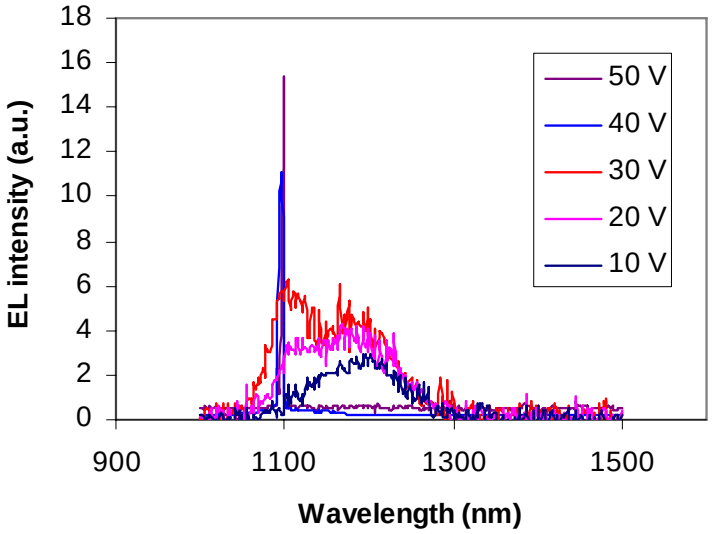

a)

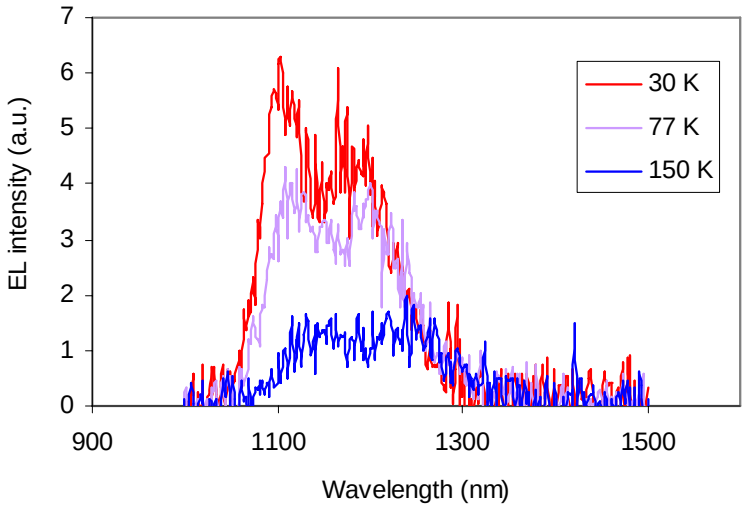

b)

Fig. 13 a) sample a-5210NSL 30K EL spectrum and b) temperature dependence of EL spectrum at fixed drive current.

Higher Sb content GaAsSb using TEGa and TESb sources

- Demonstrated 2.85nm GaAsN (4%)/2.85nm GaAsSb (38%)
- Tg=500^{o}C
- Monolayer abrupt interfaces

First demonstration of high Sb content Type-II structures on GaAs substrate

Emission wavelength ~ 1.8 μm at 30K

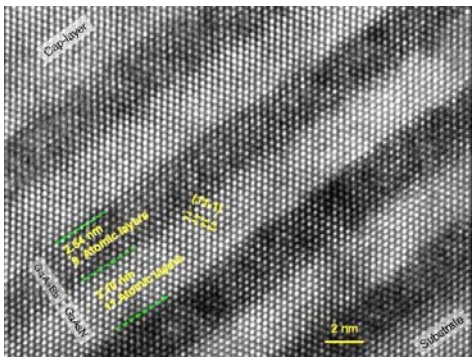

TEM micrograph

Fig. 14 demonstration of high Sb content W-structures using alternate sources.

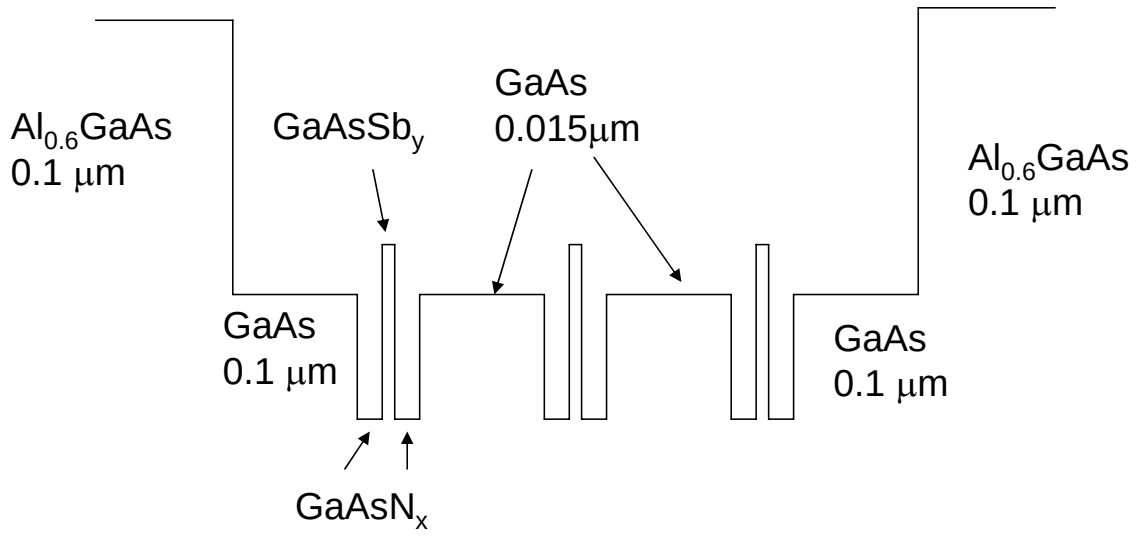

Fig. 15 Structure design for PL comparison of high Sb-content structures.

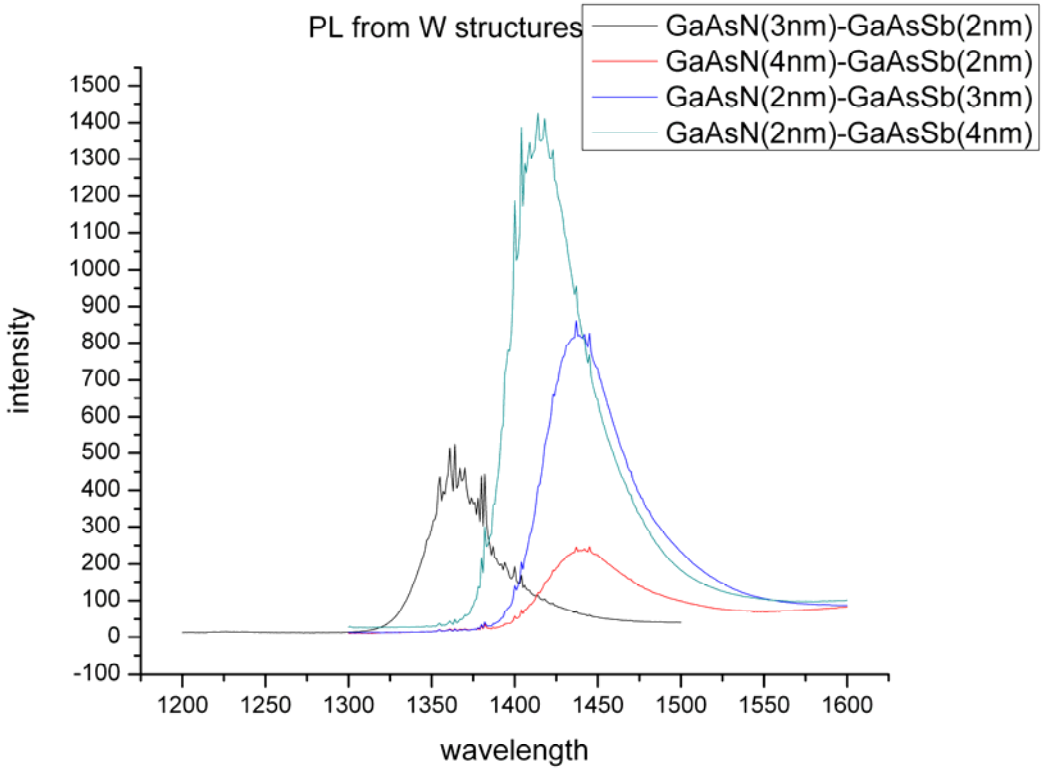

Fig. 16 LT PL from 4 different high Sb W structures as described in the legend and fig. 15.